Korean J. Chem. Eng., 39(8), 2252-2262 (2022)
DOI: 10.1007/s11814-022-1078-3

pISSN: 0256-1115
eISSN: 1975-7220

Experimental and numerical investigation of bubble nucleation and growth in supercritical CO_2-blown poly(vinyl alcohol)

Hamidreza Azimi*,†, Davoud Jahani, Sogand Aghamohammadi*, and Mohammadreza Nofar***,†**

*Department of Chemical Engineering, Faculty of Engineering, Azarbaijan Shahid Madani University, Postal Code 53751-71379, Tabriz, Iran
**Department of Mechanical Engineering, University of Bonab, P. O. Box 55517-61176, Bonab, Iran
***Sustainable & Green Plastics Laboratory, Metallurgical & Materials Engineering Department, Faculty of Chemical and Metallurgical Engineering, Istanbul Technical University, Istanbul, 34469, Turkey
(*Received 10 November 2021 • Revised 25 January 2022 • Accepted 27 January 2022*)

Abstract−Bubble nucleation and growth was experimentally and numerically investigated in polyvinyl alcohol (PVA) while using supercritical carbon dioxide ($scCO_2$) as a blowing agent. The solubility and diffusivity of CO_2 in PVA were first evaluated using a magnetic suspension balance (MSB). Bubble nucleation and growth during foaming was then examined using a batch foaming setup equipped with a visualization system. It was observed that the increase in depressurization rate during the foaming increased the average bubble density. The average bubble size during the foaming was also evaluated through three different numerical models based on the integral method. Moreover, according to the bubble pressure profile, the PVA viscosity and CO_2 diffusion control the bubble growth. According to the sensitivity analysis, the bubble growth seems to be more affected by the changes of thermodynamic parameters than the PVA rheological properties. Eventually, the average CO_2 concentration and the critical free energy were numerically calculated using the classic nucleation theory.

Keywords: Polyvinyl Alcohol (PVA), CO_2, Solubility, Diffusivity, Foaming, Visualization, Simulation

INTRODUCTION

Microcellular polymer foams refer to the class of lightweight materials with bubble sizes of 1 to 50 μm. According to such fine bubble morphological characteristics, these foam structures possess superior mechanical properties such as high specific strength and toughness [1-3]. In microcellular foaming of thermoplastics blown with physical blowing agents, several parameters, such as blowing agent type, saturation pressure, and the applied thermodynamic instability could determine the final bubble density, size, and growth rate [3,4]. The solubility and diffusivity of various blowing agents in thermoplastics are different [5-8]. This influences the bubble nucleation and growth rate through the changes in pressure drop rate and the applied thermodynamic instability [1,9-11]. The changes in saturation pressure of an identical blowing agent could also affect the pressure drop rate and the degree of applied thermodynamic instability and hence the noted bubble characteristics [12-15]. On the other hand, thermodynamic instability, which causes bubble nucleation and growth, could be provided through either a sudden pressure release or temperature increase [4,9,16-19]. During this step, nucleated bubbles can be stabilized when the bubble radius reaches the critical value [20-22]. Moreover, bubble nucleation and growth, and hence the final cellular structure of the foamed product, are dependent on the material's characteristics. Surface tension, rheological properties and crystallization behavior of the used polymer as well as the incorporation of additives such as micro-/nano-sized particulates could also noticeably influence the bubble nucleation and growth rate and the bubble stability [23-26].

The simulation of bubble nucleation and growth during foaming has been explored in a series of studies [10,19,27-29]. Gent and Tompkins [30] visualized the foaming process of a cross-linked elastomer/carbon dioxide (CO_2) and reported the changes in bubble radius with foaming time. Using a visualization apparatus, Amon and Denson [31] compared the transient foam bulk density with the simulation values. Han and Yoo [32] also developed a molding process for foaming of polystyrene with different injection rates in foam extrusion through a converging die and they compared the experimental and numerical data. A bubble growth model was developed by Payvar et al. [33] according to the mass transfer-controlled integral method. They showed that the predicted results were consistent with foaming experimental data for ethyl alcohol [33]. Ramesh et al. [34] investigated the mathematical simulation for the heterogeneous nucleation of microcellular foams. They investigated the bubble nucleation and growth dependency on various parameters such as the saturation temperature and pressure, concentration of nucleating agents and blowing agent solubility. Shafi et al. [35] also developed a simultaneous model for bubble nucleation and growth. They considered a cluster which could be nucleated when it reaches a supercritical state. A nucleation rate equation could also be generated while the bubble nucleation is derived from classical nucleation theory [35]. Some researchers extended Shafi's model to viscoelastic fluid systems [36] or to foam extrusion pro-

†To whom correspondence should be addressed.
E-mail: h.azimi@azaruniv.ac.ir, nofar@itu.edu.tr

cesses [37]. The nucleation and growth of bubbles in non-Newtonian and Newtonian fluids were studied by Frank et al. [38]. The visualization results showed that the bubbles grow linearly with time, although after a critical radius the size increase continues exponentially [38]. Ishikawa et al. [39] worked on numerical studies of polypropylene foaming blown with CO_2. They used a visualization chamber and analyzed the bubble nucleation and growth during the foaming process. Similar work was conducted in extrusion foaming of polystyrene blown with CO_2 [40] where the saturated system was subjected to a rapid pressure drop at the die. Another simulation model for foaming process was also proposed by Sun et al. [41] in which the concentration boundary layers overlapping was used in the model and the effects of physical properties of the polymer matrix on the foaming process were explored. Riou et al. [42] compared the numerical and experimental results using a growth model while considering the melt rheology effects on foaming.

In this study, the solubility and diffusivity of $scCO_2$ in PVA were first evaluated using a magnetic suspension balance (MSB). The bubble nucleation and growth in PVA/CO_2 mixture were then investigated using a batch foaming setup equipped with a visualization system. The average bubble radius and density versus time were then plotted and analyzed for various depressurization rates. The bubble nucleation and growth were also simulated using three different numerical models of Han and Yoo [32], Payvar [33] and Shafi [35]. These models were developed for solving the diffusion equation of CO_2 in PVA. The effect of various simulation variables on bubble growth was subsequently explored through sensitivity analysis. The Gibbs free energy and average concentration of CO_2 were eventually calculated according to classic nucleation theory.

EXPERIMENTAL

1. Material

PVA with weight average molecular weight of 90,000 g/mol and a hydrolyse grade of 98.7% was supplied from Kuraray, Japan. The melting temperature (T_m) of PVA, which was obtained through differential scanning calorimetry (DSC, Netzsch-DSC200 F3 Maia) analysis, was determined to be 194 °C. A rheological analysis of PVA was conducted using an MCR 301 rheometer (Anton Paar, Austria), and it was seen that PVA shows shear thinning behavior. CO_2 was used as the blowing agent. To generate the supercritical phase, CO_2 gas was pressurized using a plunger pump (Isco 260D, USA).

2. Characterization Experiments

Solubility and diffusivity of CO_2 in PVA were evaluated using

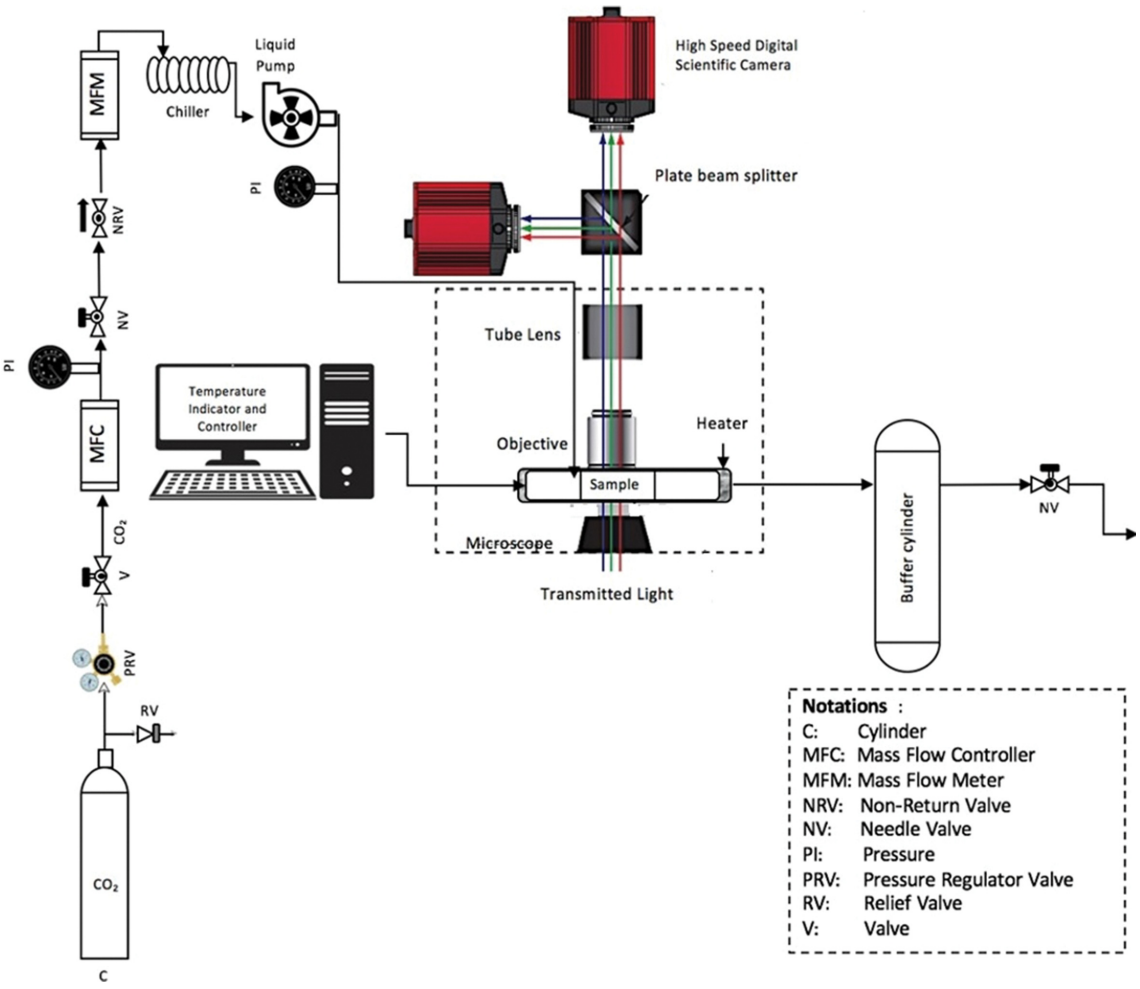

Fig. 1. Schematic of the visual observation batch foaming setup.

an MSB apparatus. The details of the measurements are provided in previous studies [11,43]. Foam visualization was also conducted using a lab-scale batch foaming setup which was connected to the Bell view software. The schematic of this visual foaming setup is shown in Fig. 1. This system has a visual observation chamber made of high-pressure stainless steel. The CO_2 is supplied to the chamber through a mass flow meter. The chamber temperature is also tailored using a heat controller. The sapphire window on the chamber together with a high-speed digital camera was designed to visualize the bubble nucleation and growth. The foaming and foam visualization of PVA was conducted during the depressurization step. The recorded bubble nucleation and growth were then analyzed using image processing software.

3. Bubble Growth Modeling

The governing equation for a single bubble growth in a polymer melt solution can be presented by three equations based on an overall force balance on the melt, mass balance of the gas in the polymer melt and the mass balance on the bubble. Fig. 2 represents the schematic of a single bubble growth with blowing agent in which pressurized blowing agent diffuses into the polymer matrix. Initial concentration of diffused blowing agent in molten polymer, C(0), is given by Eq. (1):

$$C(0) = K_{\mathcal{H}} P_G \tag{1}$$

where P_G is the bubble pressure and $K_{\mathcal{H}}$ solubility parameter being proportional to the attributed Henry's constant. Note that far-field pressure, P_L, can be obtained from saturation pressure at initial time (t=0). Blowing agent supersaturation state is provided after far-field pressure release resulting in the value of $P_G - P_L(t)$ being higher than zero.

Blowing agent diffusion has been taken into account by the gas bubble-polymer interface. The shape of the bubble seems to be spherical. The ideal gas equation was used for supercritical CO_2. Newtonian behavior was assumed during the whole foaming process.

A combined equation of momentum and continuity of the melt surrounding the bubble in the radial component (r) of spherical coordinate gives:

$$\frac{dR}{dt} = \frac{R}{4\eta}\left(P_G - P_L - \frac{2\sigma}{R}\right) \tag{2}$$

where, η is the viscosity, and σ is the surface tension, R is the bubble radius, P_G and P_L are the bubble pressure and the ambient pressure, respectively. Mass balance of the bubble requires that the rate of mass added to the bubble by blowing agent diffusion equals the rate that the gas diffuses in through the bubble surface. Thus, the diffusive mass balance at the bubble surface relates bubble pressure to the concentration gradient at the surface:

$$\frac{d}{dt}\left(\frac{4\pi R^3 P_G}{3 \mathcal{R}_g T}\right) = 4\pi R^2 D \frac{\partial C}{\partial r}\Big|_{u_{r=R}} \tag{3}$$

The ordinary differential form of bubble pressure is:

$$\frac{dP_G}{dt} = 3D(\mathcal{R}_g T)\frac{1}{R}\frac{\partial C}{\partial r}\Big|_{u_{r=R}} = 3\frac{P_G}{R}\frac{dR}{dt} \tag{4}$$

where T is the absolute temperature and $\mathcal{R}_g$ is the gas constant. Diffusion of gas in the melt is assumed to obey Fick's law defined as

$$\frac{\partial C}{\partial r} = D\left[\frac{1}{r^2}\frac{\partial}{\partial r}\left(r^2\frac{\partial C}{\partial r}\right)\right] \tag{5}$$

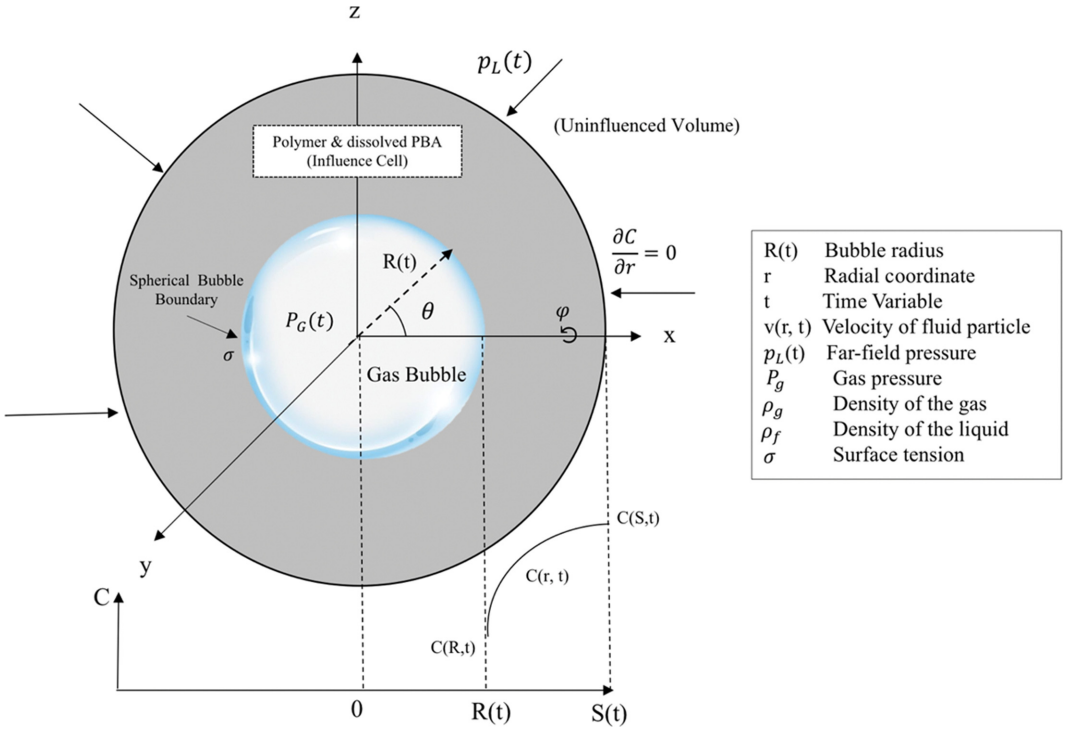

Fig. 2. Schematic of a single bubble growth with blowing agent.

In Eq. (5), C is the CO_2 concentration and D is the CO_2 diffusion coefficient. Eq. (5) describes the concentration profile in the polymer melt. Eq. (5) is indeed expressed by integrating the polynomial profile. This profile is illustrated in Fig. 2. In this study, while the Han and Yoo, Payvar and Shafi models (based on the integral method) were used, the finite difference [27] and integral [32,33] methods were used for solving Eq. (5).

To know the concentration gradient at the bubble-melt interface for Eq. (3), the below three different numerical models were used in this study.

1. Han and Yoo model:

$$\frac{d}{dt}(R^3P_G)=\frac{6D(\mathcal{R}_gT)(C_\infty-C_R)R}{-1+\left\{1+\frac{2/R^3}{\mathcal{R}_gT}\left(\frac{R^3P_G-R_0^3P_{G,0}}{C_\infty-C_R}\right)\right\}^{1/2}} \tag{6}$$

$$\frac{C_\infty-C}{C_\infty-C_R}=\left(1-\frac{r-R}{\delta}\right)^2 \tag{7}$$

2. Payvar model:

$$\frac{d(R^3P_G)}{dt}=3D(\mathcal{R}_gT)(C_\infty-C_R)R\left[1+\frac{1}{-1+\left\{1+\frac{2/R^3}{\mathcal{R}_gT}\left(\frac{R^3P_G-R_0^3P_{G,0}}{C_\infty-C_R}\right)\right\}^{1/2}}\right] \tag{8}$$

$$\frac{C_\infty-C}{C_\infty-C_R}=\frac{R}{r}\left(1-\frac{r-R}{\delta}\right)^2 \tag{9}$$

3. Shafi model:

$$\frac{d}{dt}(R^3P_G)=\frac{36}{5}\frac{R^4(\mathcal{R}_gT)(C_\infty-C_R)^2}{R^3P_G-R_0^3P_{G,0}} \tag{10}$$

$$\frac{C_\infty-C}{C_\infty-C_R}=\frac{r^3-R^3}{(R+\delta)^3-R^3} \tag{11}$$

In the above models one parameter was used for identifying the boundary thickness. This parameter is named δ according to Fig. 2. The initial conditions of bubble radius and bubble pressure are as follows:

$$R(t_n)=\frac{2\sigma}{\overline{C}/k_H-P_L} \tag{12}$$

$$P_G(t_n)=\overline{C}/k_H \tag{13}$$

Due to the importance of foaming thermodynamics, the critical free energy and the average CO_2 concentration were determined according to classical nucleation theory:

$$J(t)=f_0\left(\frac{2\sigma}{\pi M_w/N_A}\right)^{1/2}\exp\left(\frac{\Delta G}{K_BT}\right)N_A\overline{C}(t) \tag{14}$$

$$\Delta G=\frac{16\pi\sigma^3F}{3\left(\frac{\overline{C}(t)}{k_H}-P_L(t)\right)^2} \tag{15}$$

Differentiating above equation by t gives:

$$\left(\frac{d\Delta G}{dt}\right)=\left(\frac{-32\sigma^3F}{3\left(\frac{\overline{C}(t)}{k_H}-P_L(t)\right)^3}\right)\left[\frac{d\left(\frac{\overline{C}(t)}{k_H}\right)}{dt}-\frac{dP_L}{dt}\right] \tag{16}$$

where f_0 and F are fitting parameters of nucleation rate and ΔG is the critical free energy of bubble nucleation. This energy is a kind of obstacle for starting the bubble nucleation, and when it is overcome bubble nucleation starts. N_A is Avogadro's number, k_B is Boltzmann's constant, and M_w is the molecular weight of blowing agent.

The average concentration of CO_2 in PVA with the volume of V_{L0} is given by:

$$\overline{C}(t)V_{L0}=C_0V_{L0}-\int_0^t\frac{4\pi}{3}R^3(t-t_n,t_n)\frac{P_G(t-t_n,t_n)}{\mathcal{R}_gT}J(t_n)V_{L0}dt_n \tag{17}$$

In the above equation, t is the time that a bubble nucleates and $t-t_n$ is the period in which a single bubble grows. Bubble nucleation

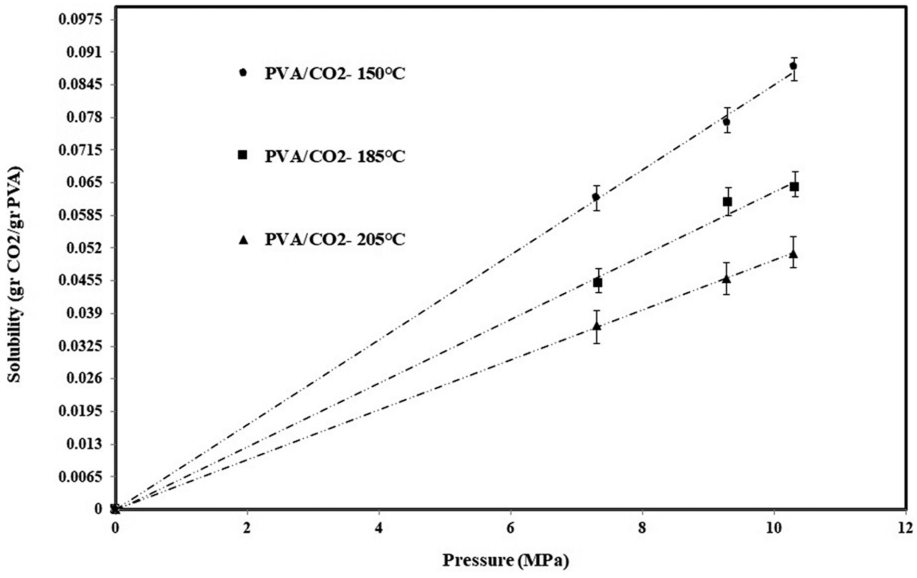

Fig. 3. Solubility of CO_2 in PVA at different temperatures and pressures.

starts when the bubble nucleation rate (J) becomes greater than the bubble nucleation rate threshold ($J_{threshold}$).

RESULTS AND DISCUSSION

1. CO_2 Solubility and Diffusivity in PVA

Fig. 3 shows the solubility behavior of CO_2 in PVA at various pressures and temperatures. As expected, the CO_2 solubility in PVA increases with pressure increment due to the pressure driving force for dissolution of CO_2 in PVA. This is while the solubility has an opposite trend with temperature increment. With temperature increase, the CO_2 molecules evacuate the PVA matrix and hence the CO_2 solubility decreases. The CO_2 diffusion coefficients in PVA with pressure, at different temperatures, are also shown in Fig. 4. Diffusion coefficients are increased by increasing of the temperature and pressure.

2. Foam Visualization

To run the foaming experiments, the samples were first saturated at 185 °C and CO_2 pressure of 9.6 MPa. The foaming and the bubble nucleation and growth visualization were then conducted during the depressurization step, which was separately conducted at three different depressurization rates of 3.47, 1.24, and 0.52 MPa/s. The recorded micrographs during the foaming and depressurization at the rate of 0.52 MPa/s are shown in Fig. 5. According to

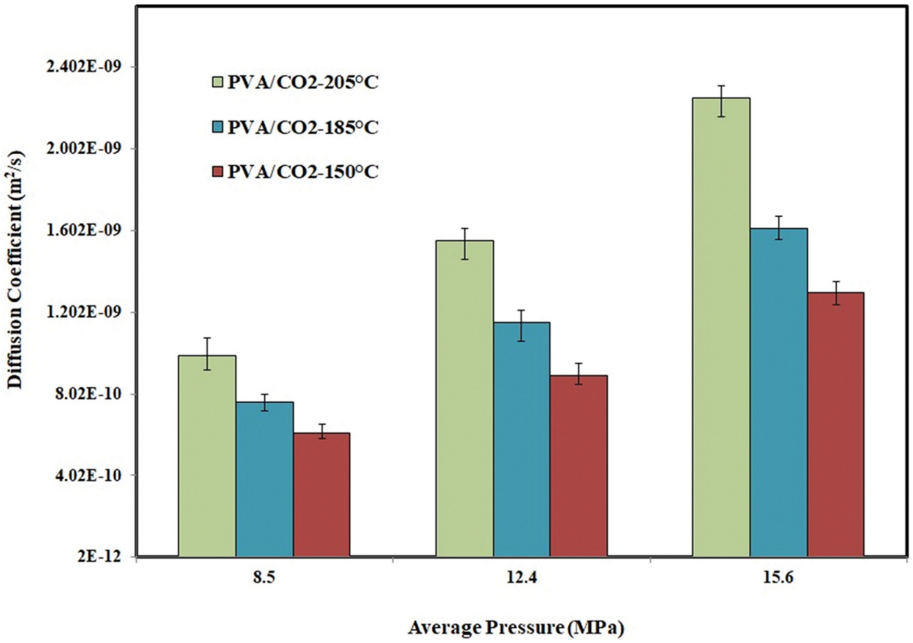

Fig. 4. Diffusion coefficient of CO_2 in PVA at different temperatures and pressures.

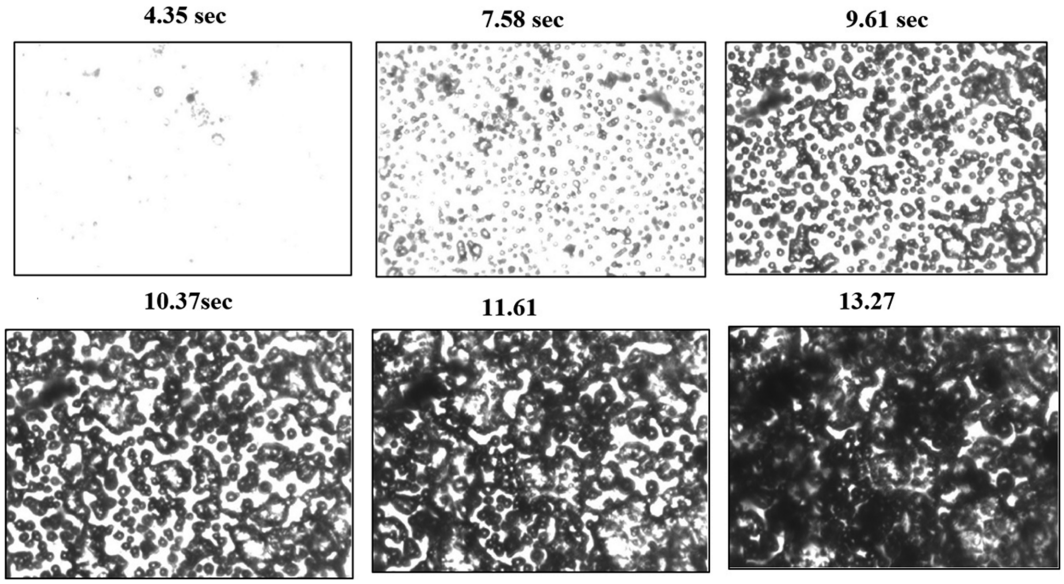

Fig. 5. Optical micrographs recorded during foam visualization at pressure release rate of 0.52 MPa/s.

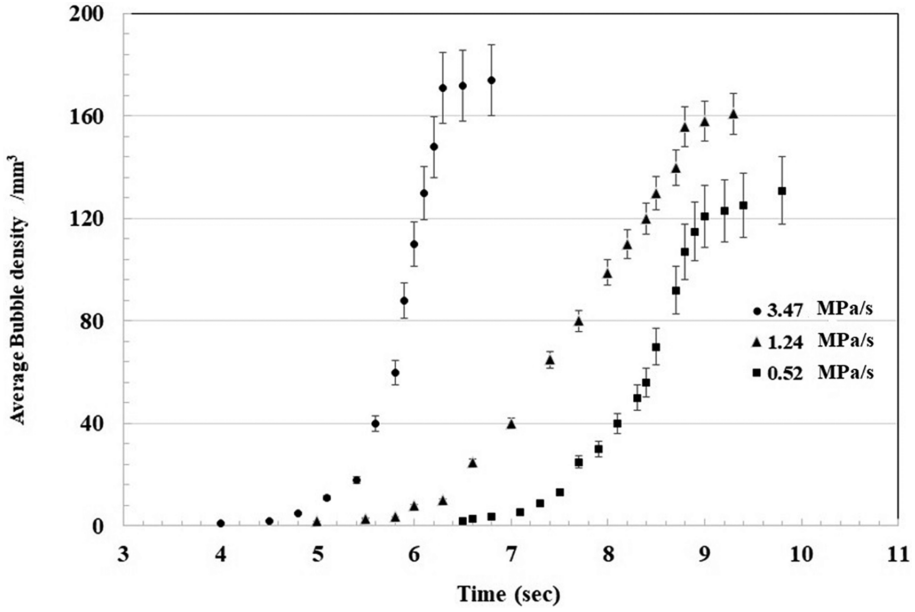

Fig. 6. Effect of CO_2 pressure release rate on the average bubble density of PVA.

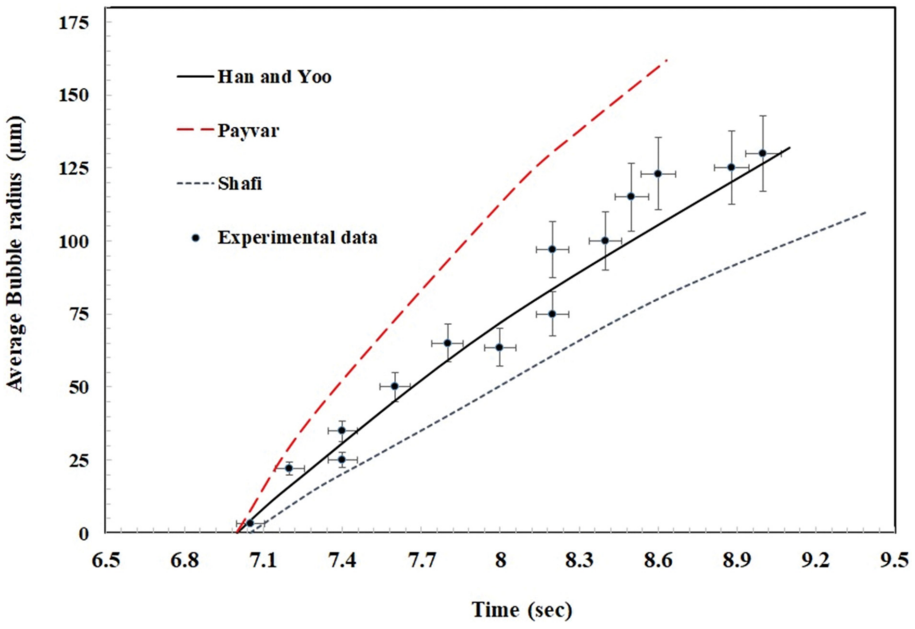

Fig. 7. Experimental data and simulated results at pressure release rate of 0.52 MPa/s.

these images, the bubble density and growth could be determined at certain foaming times. The average bubble density in three pressure release rates versus time is illustrated in Fig. 6. As expected, the average bubble density increased with the increased pressure release rate. This indicates that the pressure release rate significantly controls the average bubble density. At higher pressure release rates, the accessible CO_2 for diffusing into the nucleated bubbles in PVA increases during the foaming and hence the bubble growth could occur faster.

3. Bubble Growth Simulations

The accuracy and validation of experimental data were investigated through simulation studies and the corresponding numerical values are reported in this section through using the models developed by Han and Yoo, Payvar, and Shafi. Figs. 7-9 compare the average bubble radius values versus time at different pressure release rates obtained through using the noted models. As shown, the Han and Yoo model could more accurately predict the bubble growth behavior. Considering the Shafi and Payvar models, it seems that the bubble growth rate is either slow or fast, respectively. According to Fig. 9, however, it seems that the experimental data at higher pressure drop rate could also be predicted by Payvar model, although the compatibility of the experimental data with Han and

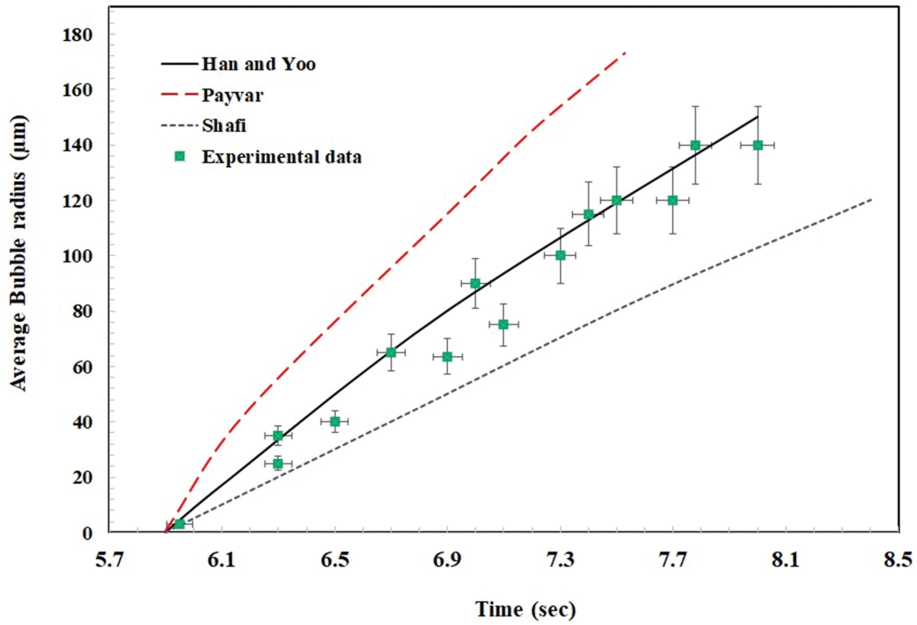

Fig. 8. Experimental data and simulated results at pressure release rate of 1.24 MPa/s.

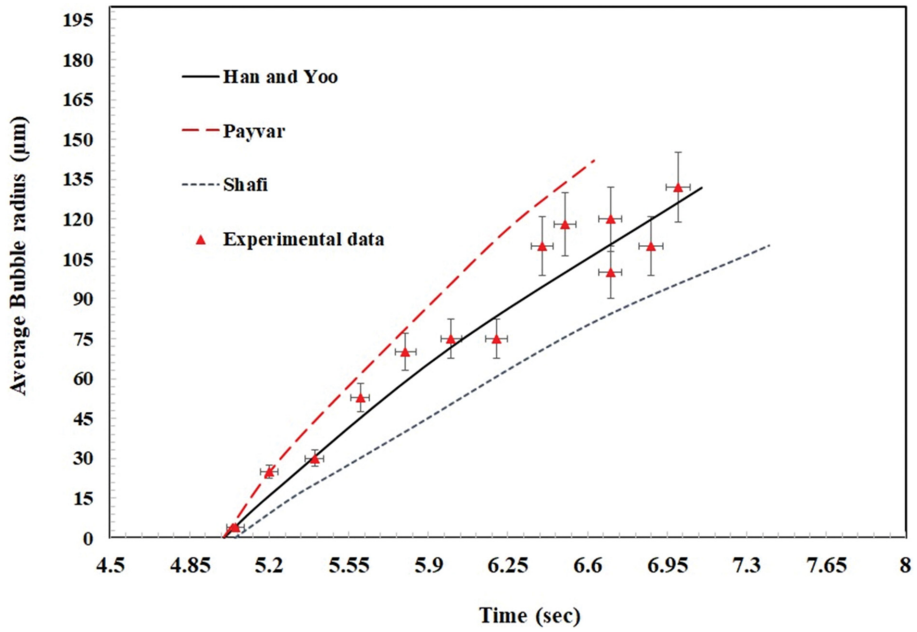

Fig. 9. Experimental data and simulated results at pressure release rate of 3.47 MPa/s.

Yoo model is still better. Fig. 10 also depicts the bubble pressure versus time during the foaming. As seen, during the bubble growth, the pressure profile of the bubble undergoes two different states. The bubble pressure after a short interval of about 0.3 s (region 1) starts decreasing during the foaming step (region 2). Thus, in region 1, bubble nucleation occurs during a short interval of about 0.3 s during which the change in bubble radius is slow. This is because when bubble nucleation starts, the bubble pressure and the saturation pressure are similar, indicating that the concentration gradient at PVA/CO_2 interface of bubble is almost zero. Such behavior is highly dependent on the polymer's viscosity. Hence, such time interval of region 1 could prolong with the increase in matrix viscosity. In region 2, the bubble pressure keeps decreasing to reach the ambient pressure. In this region, CO_2 diffuses into bubbles and is consumed by the growing bubbles. Therefore, the concentration gradient at the PVA/CO_2 interface is much larger than region 1. This means that the bubble growth is majorly dominant in region 2.

According to Figs. 7-9, the Han and Yoo model was selected to further investigate the effect of various simulation variables on bubble growth through sensitivity analysis in Fig. 11. For instance, to consider the solubility effect, the use of different values for the Henry constant (solubility parameter) resulted in curves with dif-

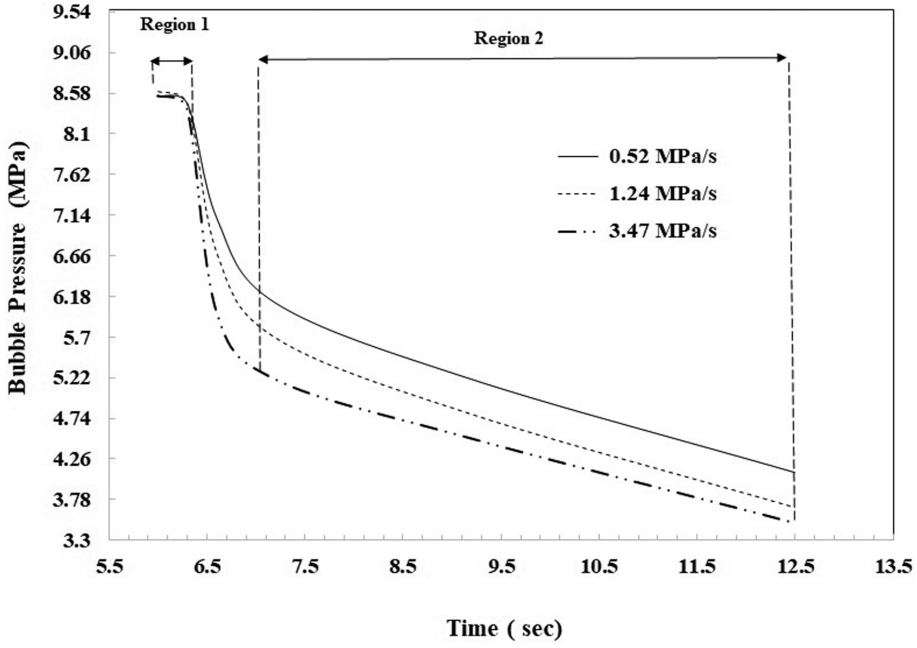

Fig. 10. Bubble pressure profile versus foaming time at different pressure release rates.

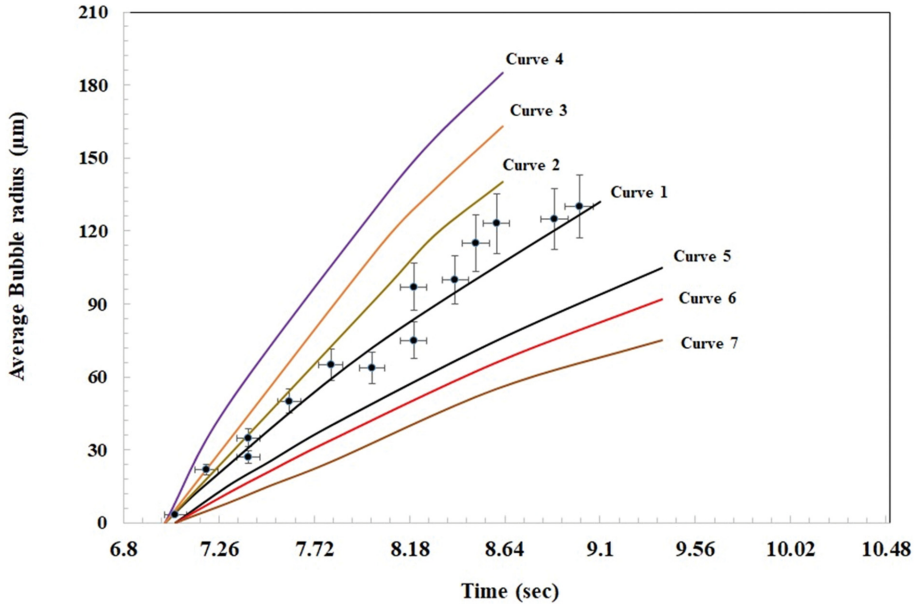

Fig. 11. Effect of numerically changing different parameters according to the Han and Yoo model, on the bubble growth at pressure release rate of 0.52 MPa/s.

ferent bubble radius values versus foaming time. Similar investigations were conducted for diffusivity and viscosity as the changing parameters. Hence, various bubble growth profiles could be obtained depicting the individual effects of solubility, diffusivity and viscosity on foaming dynamics.

As shown in the Fig. 11, the curve related to the Han and Yoo model is plotted using the measured parameters in this study. For example, according to the sensitivity analysis shown in Fig. 11 and Table 1, when the viscosity, as a rheological parameter, increases nearly sixty times, the final bubble size decreases 1.3 times and the corresponding curves (curves 2 and 5 in Fig. 11) become close to the experimental data. The viscosity increase hinders the bubble growth and the growth rate decreases. However, when the Henry constant is doubled or the diffusion coefficient increases 2.5 times, the final bubble size increases more than 2 times and the relevant curves are significantly far from each other. A larger CO_2 solubility parameter (k_H) means that the PVA can dissolve more CO_2 molecules and larger bubbles are expected. Moreover, the higher diffusivity causes the CO_2 molecules to diffuse to the nucleated bubbles faster, which increases the bubble growth rate. This indicates that

Table 1. The sensitivity analysis for the PVA/CO_2 foaming using Han and Yoo model

Curve number	k_H (mol/m^3/Pa)	D (m^2/s)	μ (Pa·s)	Final Bubble radius (μm)
1	0.0064	8.11×10^{-10}	5.1×10^{5}	132
2	0.0064	8.11×10^{-10}	2×10^{4}	140
3	0.0081	8.11×10^{-10}	5.1×10^{5}	163
4	0.0064	1.32×10^{-9}	5.1×10^{5}	185
5	0.0064	8.11×10^{-10}	1.2×10^{6}	105
6	0.0064	4.03×10^{-10}	5.1×10^{5}	92
7	0.0043	8.11×10^{-10}	5.1×10^{5}	75

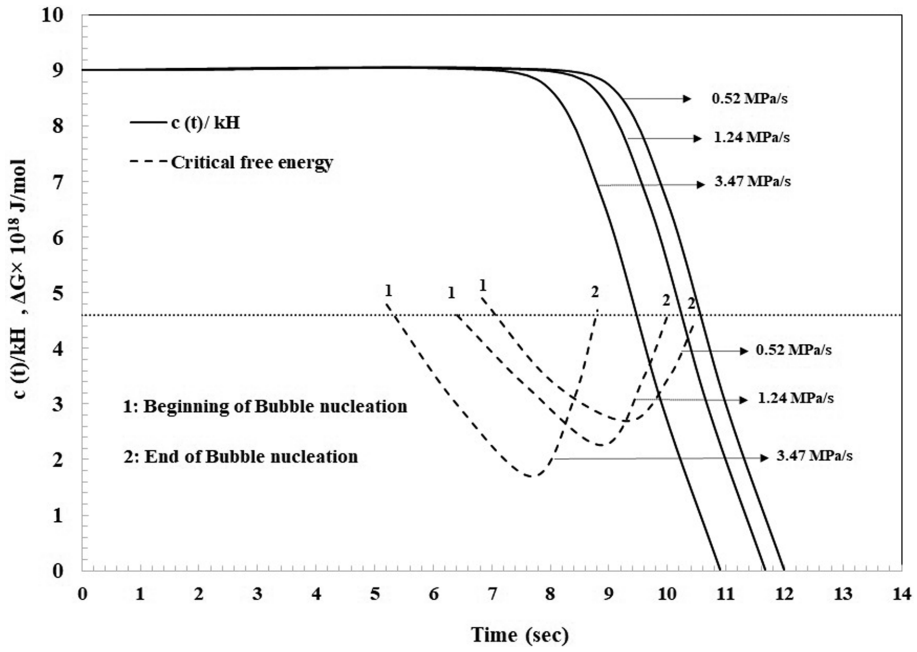

Fig. 12. Changes in average concentration and critical free energy of bubble nucleation at different pressure release rates.

bubble growth and foaming could be more affected by the thermodynamics parameters than the viscosity effect of the matrix.

According to classic nucleation theory, the average concentration of CO_2 and the free energy could be numerically calculated. To determine the parameters of f_0 and F in Eq. (14) and (15), the data in Fig. 6 was used. A trial-and-error method was used for calculating the f_0 and F parameters in which by changing different values of f_0 and F the average bubble density was fitted to the PVA/CO_2 system and the amounts of f_0 and F were calculated as 2.8×10^{-23} and 0.013121, respectively. Therefore, the critical free energy and the change in average concentration of CO_2 at 0.52. 1.24 and 3.47 MPa/s were determined, respectively, and are shown in Fig. 12. As shown, the average concentration of CO_2 remains constant up to a certain time and then decreases. Before this time, the free energy has a definite value, the ambient pressure and the supersaturation pressure reach each other, bubbles nucleate and the critical free energy decreases in the period of 4.4-10.5 seconds according to three depressurization rates. In this period, the average concentration of CO_2 is constant. Then, it decreases with time because CO_2 diffuses into the bubbles. During this period, the supersaturation pressure has a low value and is not suitable for nucleation of bubbles and then nucleation stops. The decrease in concentration increases the free energy of bubble nucleation. Therefore, in the simulation, the critical free energy has a minimum value in the time range of 4.4-10.5 s.

When the left-hand side of Eq. (16) equals zero, the critical free energy has a minimum and at this point the terms in bracket of Eq. (16) equal zero. As Fig. 12 shows, the time that the critical free energy reaches a minimum value is the same as the time that the CO_2 average concentration starts to decrease. This means that with a lower value of the minimum free energy, the beginning time of average concentration decrement was decreased and foaming process occurred earlier. Indeed, increasing of the pressure release rate increases the bubble density during the process and decreases the minimum free energy, which also is shown in Fig. 13.

CONCLUSIONS

Bubble growth visualization and simulation was done using a visual batch foaming setup for PVA/CO_2 system at three different pressure release rates. It was shown that the Han and Yoo model seems to be more consistent with the experimentally obtained val-

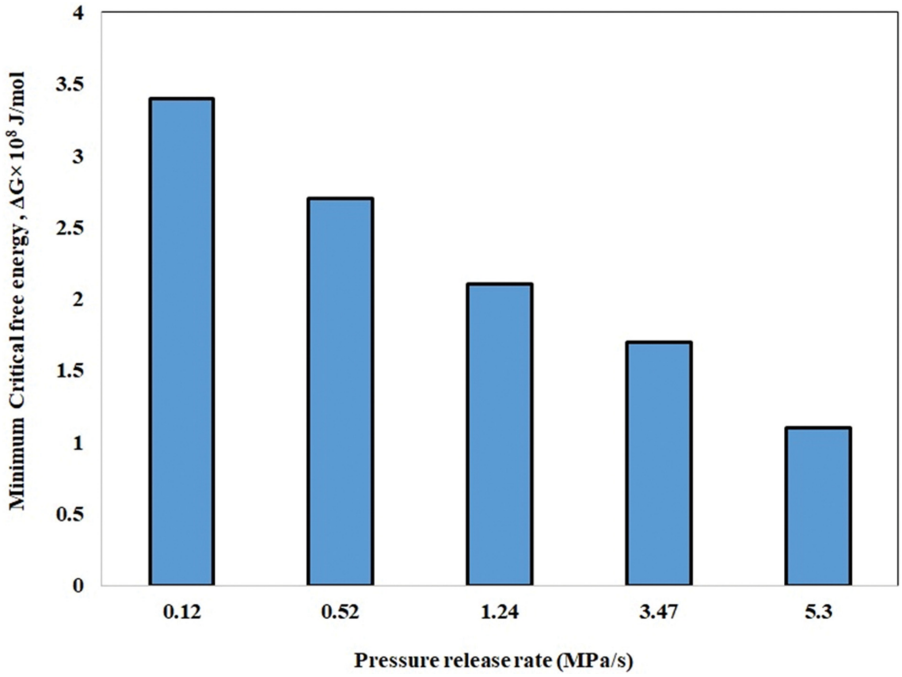

Fig. 13. The change in critical free energy versus the pressure release rate.

ues. It was also concluded that with solubility and diffusivity increment and viscosity decrement, the bubble growth rate increased although the bubble growth process seemed to be more affecting the thermodynamic parameters than the matrix rheological features. Moreover, according to the classic nucleation theory, the calculated average concentration of CO_2 and the critical free energy results show that these two parameters are correlated during the foaming.

Eventually, to explore the thermodynamics and viscosity effects on the bubble nucleation and growth of various polymers including PVC, it is important to experimentally and numerically investigate the effect of viscosity of PVC by selecting various molecular weight matrix samples. Hence, the thermodynamics and viscosity correlations on the foaming behavior of the polymer matrix could more accurately be disclosed.

ACKNOWLEDGEMENTS

The authors would like to acknowledge the Iran National Science Foundation (INSF) for the financial support of this research project with project number of 99010405.

REFERENCES

1. C. B. Park, D. F. Baldwin and N. P. Suh, *Prog. Polym. Sci.*, **35**(5), 432 (1995).
2. C. B. Park and N. P. Suh, *Prog. Polym. Sci.*, **36**(1), 34 (1996).
3. C. B. Park and L. K. Cheung, *Prog. Polym. Sci.*, **37**(1), 1 (1997).
4. M. Nofar and C. B. Park, *Polylactide foams: Fundamentals, manufacturing, and applications*, William Andrew (2017).
5. R. Li, J. H. Lee, C. Wang, L. H. Mark and C. B. Park, *J. Supercrit Fluids*, **154**, 104623 (2019).
6. Q. P. Guo, J. Wang and C. B. Park, *Int. Polym. Process.*, **35**(5), 503 (2020).
7. M. Nofar, A. Tabatabaei, A. Ameli and C. B. Park, *Polymer*, **54**(23), 6471 (2013).
8. A. Wong, L. H. Mark, M. M. Hasan and C. B. Park, *J. Supercrit Fluids*, **90**, 35 (2014).
9. M. Nofar and C. B. Park, *Prog. Polym. Sci.*, **39**(10), 1721 (2014).
10. Q. Guo, J. Wang, C. B. Park and M. A. Ohshima, *Ind. Eng. Chem. Res.*, **45**(18), 6153 (2006).
11. H. R. Azimi and M. Rezaei, *J. Chem. Thermodyn.*, **58**, 279 (2013).
12. B. Batı, E. B. Küçük, A. Durmuş and M. Nofar, *J. Polym. Eng.*, **40**(7), 561 (2020).
13. S. N. Leung, A. Wong, C. B. Park and Q. Guo, *Ind. Eng. Chem. Res.*, **48**(4), 1921 (2009).
14. M. Nofar, E. B. Küçük and B. Batı, *J. Supercrit Fluids*, **153**, 104590 (2019).
15. M. Nofar, B. Batı, E. B. Küçük and A. Jalali, *J. Supercrit Fluids*, **160**, 104816 (2020).
16. A. Nistor, M. Topiar, H. Sovova and J. Kosek, *J. Supercrit Fluids*, **130**, 30 (2017).
17. M. Keshtkar, M. Nofar, C. B. Park and P. J. Carreau, *Polymer*, **55**(16), 4077 (2014).
18. G. O. Aloku and X. F. Yuan, *Chem. Eng. Sci.*, **65**(12), 3749 (2010).
19. I. Álvarez, C. Gutiérrez, J. F. Rodríguez, A. de Lucas and M. T. García, *J. Supercrit Fluids*, **164**, 104886 (2020).
20. S. N. Leung, C. B. Park, D. Xu, H. Li and R. G. Fenton, *Ind. Eng. Chem. Res.*, **45**(23), 7823 (2006).
21. S. N. Leung, A. Wong, Q. Guo, C. B. Park and J. H. Zong, *Chem. Eng. Sci.*, **64**(23), 4899 (2009).
22. C. Wang, S. N. Leung, M. Bussmann, W. T. Zhai and C. B. Park, *Ind. Eng. Chem. Res.*, **49**(24), 12783 (2010).
23. M. Xu, J. Lu, J. Zhao, L. Wei, T. Liu, L. Zhao and C. B. Park, *Poly-*

mer, **224**, 123730 (2021).
24. M. Nofar, *Int. J. Mater. Sci. Res.*, **1**, 16 (2018).
25. H. Park, C. B. Park, C. Tzoganakis and P. Chen, *Ind. Eng. Chem. Res.*, **46**(11), 3849 (2007).
26. M. Nofar, *Mater. Des.*, **101**, 24 (2016).
27. A. Arefmanesh, S. G. Advani and E. E. Michaelides, *Int. J. Heat Mass Transf.*, **35**(7), 1711 (1992).
28. Y. Ge and T. Liu, *Chem. Eng. Sci.*, **230**, 116213 (2021).
29. H. Azimi, D. Jahani and M. Nofar, *J. Chem. Eng. Data*, **65**(9), 4596 (2020).
30. A. N. Gent and D. A. Tompkins, *Int. J. Appl. Phys.*, **40**(6), 2520 (1969).
31. M. Amon and C. D. Denson, *Prog. Polym. Sci.*, **26**(3), 255 (1986).
32. H. J. Yoo and C. D. Han, *Prog. Polym. Sci.*, **21**(2), 69 (1981).
33. P. Payvar, *Int. J. Heat Mass Transf.*, **30**(4), 699 (1987).
34. N. S. Ramesh, D. H. Rasmussen and G. A. Campbell, *Prog. Polym. Sci.*, **34**(22), 1685 (1994).
35. M. A. Shafi and R. W. Flumerfelt, *Chem. Eng. Sci.*, **52**(4), 627 (1997).
36. K. Joshi, J. G. Lee, M. A. Shafi and R. W. Flumerfelt, *J. Appl. Polym. Sci.*, **67**(8), 1353 (1998).
37. M. Shimoda, I. Tsujimura, M. Tanigaki and M. Ohshima, *J. Cell. Plast.*, **37**(6), 517 (2001).
38. X. Frank, N. Dietrich, J. Wu, R. Barraud and H. Z. Li, *Chem. Eng. Sci.*, **62**(24), 7090 (2007).
39. T. Ishikawa and M. Ohshima, *Prog. Polym. Sci.*, **51**(8), 1617 (2011).
40. S. Shukla and K. W. Koelling, *Ind. Eng. Chem. Res.*, **48**(16), 7603 (2009).
41. Y. Sun, Y. Ueda, H. Suganaga, M. Haruki, S. I. Kihara and S. Takishima, *J. Supercrit Fluids*, **107**, 733 (2016).
42. M. Riou, G. Ausias, Y. Grohens, T. Gaudry, J. M. Veillé and J. Férec, *Chem. Eng. Sci.*, **227**, 115852 (2020).
43. H. Azimi, *J. Thermoplast. Compos. Mater.*, 0892705720976192 (2020).